17th World Conference on Earthquake Engineering, 17WCEE
Sendai, Japan - September 13th to 18th 2020

A NOVEL MACRO-DISTINCT ELEMENT MODEL FOR THE IN-PLANE ANALYSIS OF UNREINFORCED MASONRY STRUCTURES

D. Malomo[1], M.J. DeJong[2]

[1] *Post-doctoral researcher, Department of Civil and Environmental Engineering, University of California, Berkeley, 760 Davis Hall, Berkeley, CA 94720; d.malomo@berkeley.edu (corresponding author)*
[2] *Assistant Professor, Department of Civil and Environmental Engineering, University of California, Berkeley, 760 Davis Hall, Berkeley, CA 94720; dejong@berkeley.edu*

Abstract

The use of Distinct Element Method (DEM) based micro-modeling strategies for simulating the response of unreinforced masonry (URM) structures has primarily focused on the analysis of local problems of arched and reduced-scale dry-joint assemblies, i.e. in cases where the number of degrees of freedom is limited and the effect of masonry material properties is usually not predominant. While DEM provides the possibility of explicitly representing damage patterns and failure mechanisms, as well as of accounting for the mechanical interaction among in-plane and out-of-plane loaded components, the computational cost is high. In this work, aimed at combining the efficiency of simplified modeling strategies with the accuracy of discontinuum-based micro-modeling approaches, the development of a novel macro distinct element model (M-DEM) for simulating the response of large-scale URM assemblies with mortared joints is presented and discussed. Shear and flexural failure modes are accounted for by zero-thickness interface spring layers, whose geometrical distribution is determined *a priori* as a function of the considered masonry bond pattern. The discretization scheme is conceived in such a way that the model can be used to simulate both in-plane and out-of-plane damage, as well as combined mechanisms. Simplified expressions are proposed for determining equivalent stiffness and strength properties of the interface spring layers that separate the macro blocks. Masonry crushing failure is modeled through homogenized Finite Element macro blocks. Further, to avoid mesh dependency, a linearized version of the Feenstra compression model, typically employed in the field of concrete fracture mechanics, was implemented. The use of the proposed modeling strategy is demonstrated through an initial application, involving comparisons against experimental static tests on full-scale URM components, subjected to in-plane shear-compression loading cycles. Preliminary results indicate that the model can satisfactorily reproduce the load-displacement curves and the in-plane hysteretic responses in a reasonable timeframe, as well as the experimentally-observed failure mechanisms.

Keywords: macroelement, Finite-Distinct Element Method, in-plane, cyclic, unreinforced masonry

1. Introduction

Simplified macro-models have been used to adequately reproduce the in-plane-governed response of both full-scale and reduced-scale URM structures at relatively low computational cost (e.g. [1,2]). Despite a few recent upgrades to this original scheme have been lately proposed to consider out-of-plane actions (e.g. [3,4]), the explicit representation of the interaction between in-plane and out-of-plane-loaded members using macro-element models is still an open challenge. On the other hand, the employment of more advanced detailed models, naturally suitable for simulating collision and separation phenomena at the micro-level, typically requires a substantial increase in analysis time. In the framework of discontinuum-based micro-modeling techniques, of which a comprehensive literature review can be found in e.g. [5], the Distinct Element Method (DEM), based on the mechanical interaction among discrete bodies connected to each other through interface joint springs and originally developed by Cundall in 1971 [6], has proved to be appropriate for the analysis of URM structures [7–9], particularly in the case of arched [10] and reduced-scale dry-joints systems [11], i.e. where the effect of masonry crushing is not predominant. Indeed, compressive joint failure is not included in typical DEM formulations. For this reason, and because of the high computational expense typically required, very few applications concerning the DEM modeling of full-scale mortared-joints structures subjected to in-plane loading are documented in literature, and in most of these cases, no experimental comparisons are provided. In this paper, aimed at combining the efficiency of simplified modeling strategies with the advantages of DEM-based methods, a new Macro-Distinct Element Model (hereinafter referred to as M-DEM), is preliminarily validated against laboratory tests on full-scale piers subjected to in-plane cyclic loading. According to the M-DEM, compressive failure is accounted for by homogenized FE blocks, to which the mass of the system is assigned, while flexural and sliding/diagonal shear phenomena are represented through equivalent interface spring layers. Their layout, as extensively discussed in the body of the paper, is determined a priori as a function of the masonry texture (whose effect on the in-plane response can be accounted for numerically), also allowing the possibility of capturing out-of-plane failure modes, under both one-way and two-way bending conditions. The new approach is implemented within the 3DEC commercial software framework [12], and might also be of interest to both practitioners and researchers. Further, the explicit time-integration scheme on which the selected computational platform is founded makes this model compatible with large-displacement and collapse analysis.

2. M-DEM modeling strategy

In the framework of M-DEM, each URM member is idealized an assembly of six deformable FE macro-blocks, characterized by an internal tetrahedral mesh, connected to each other by means of nonlinear spring layers, whose number and configuration depend on the aspect ratio of the considered URM components.

In the case of an isolated URM panel as in Fig. 1(a), the layout of the spring layers is pre-determined as a function of the masonry texture. More specifically, the average slope (φ) of the lines connecting consecutive head joints along the height/length of a given masonry element [13], is used to define potential failure planes for the development of discrete cracks between the FE blocks. Such a simplified discretization scheme has been conceived in order to reproduce the main failure modes typically observed during experimental tests on both URM spandrels and URM wall components [14,15].

In the M-DEM framework, shear and tensile failures are accounted for by the interface springs, characterized by a Mohr-Coulomb criterion (no shear softening) with tension cut-off and to which normal (k_n) and tangential (k_s) dummy stiffnesses are assigned. While friction angle ϕ, cohesion c and tensile strength f_t of horizontal joints are assumed equal to those inferred through triplet and bond wrench tests respectively, equivalent values (i.e. $\bar{\phi}, \bar{c}, \bar{f}_t$) are calculated for the diagonal joints as a function of φ, using Eqs. (1), (2), (3) (see Fig. 1(b)). On the other hand, the equivalent shear/tensile strength parameter (i.e. $\bar{\bar{c}} = \bar{\bar{f}}_t$, Eq. (4)) proposed by [16], evaluated also considering the resistance provided by interlocking units (with thickness t_u, length l_u and width w_u), is specified for the t_j-thick vertical joints.

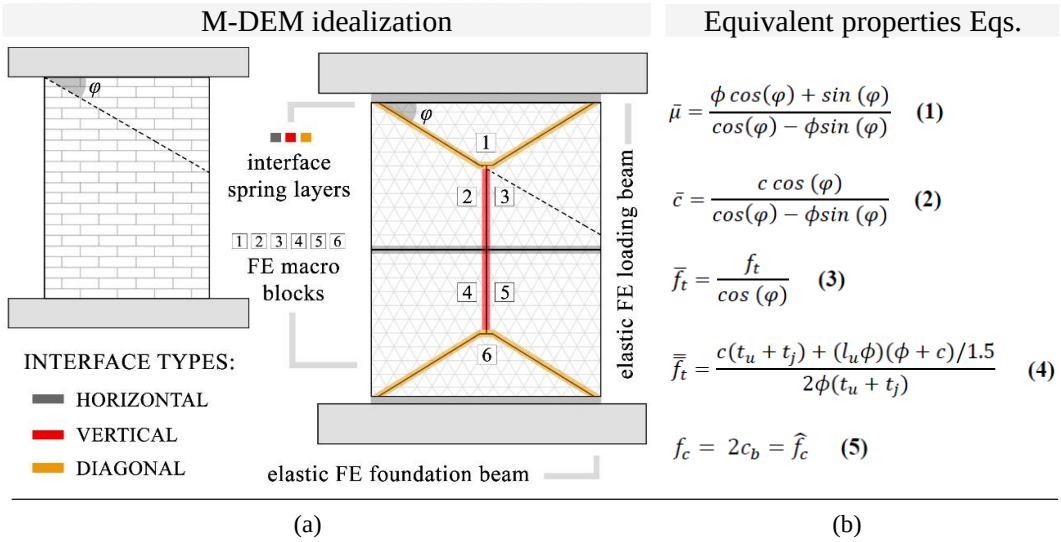

Fig. 1 (a) A Macro-Distinct Element representative of a URM panel

A linearized version of the strain-softening compression model in [17], initially conceived for simulating concrete failure, was implemented in 3DEC and assigned to the FE blocks to account for masonry crushing. To this end, assuming that the internal block friction angle ϕ_b is equal to zero, a simple correlation of block fictitious cohesion c_b to uniaxial experimental strength in compression f_c of masonry can be obtained [18], as shown in Eq. (5).

3. Validation with experimental in-plane cyclic tests on full-scale specimens

Two reduced-scale double-wythe (English bond pattern, $\varphi \simeq 28$) clay brick masonry were tested under fixed-fixed boundary conditions and quasi-static in-plane cyclic loading at the Joint Research Center (Ispra, Italy) by Anthoine et al. [18]. The main dimensions of the specimens (i.e. length L_w, height H_w and thickness t_w), hereinafter referred to as HW (i.e. high-wall) and LW (i.e. low-wall), are depicted together with the associated aspect ($\lambda_w=H_w/L_w$) and shear-span ($\alpha_v=H_0/L_w$, with $H_0=0.5H_w$) ratios in Fig.2(a). A constant vertical overburden stress σ_0 of 0.6 MPa was applied to the walls, resulting an axial load ratio of $\sigma_L=\sigma_0/f_c$. In the case of the HW panel, whose response was mainly governed by flexural-rocking, with cracks propagating through the mortar joints of both the top and bottom brick courses, two cycles were performed at each lateral displacement amplitude (see Fig.2(b)). The test was stopped at a measured displacement of circa 13 mm, i.e. 0.65% drift. An analogous loading protocol was adopted for LW, albeit three cycles per amplitude were imposed in the second-to-last test phase (i.e. after noticeable strength degradation was detected). Prior to the end of the test, the wall sustained an additional displacement cycle (see Fig.2(c)), thus reaching an ultimate displacement capacity of approximately 8 mm (i.e. 0.60% drift) and exhibiting a clearly-identifiable diagonal shear failure mechanism (which started at 0.2% drift, involving cracks through both bricks and mortar joints).

The test setup consisted of a top steel beam, to which both vertical pressures and horizontal displacement histories were applied, and a bottom reinforced concrete - RC - foundation, both rigidly connected to the walls' extremities. In the corresponding M-DEMs, the test setup has been idealized using linear elastic beam elements, representing both top beam and RC foundation.

The panel discretization was tailored on the masonry used in the experiments. In more detail, as it can be gathered from Fig.2(d), a φ-based diagonal joint inclination of 28° was adopted. Additionally, two short horizontal joints (of length 50 mm, i.e. $0.25w_u$) were introduced between the diagonal joints and the central vertical joints, to avoid potential stress localizations and early failure. This results in 1.0 m and 0.4 m long central vertical joints for HW and LW wall specimens respectively.

The experimental mechanical properties are reported in Table 1 together with those inferred analytically using the Eqs. (1)-(5), where G_c is fracture energy in compression and G_m stands for masonry shear modulus (derived assuming material isotropy, i.e. G_m =0.4E_m.

Table 1 Measured masonry material properties and equivalent parameters assigned to either springs or FE blocks

	E_m	G_m	k_n	k_s	f_c	f_t	c	ϕ	φ	$\bar{f}_t$	$\bar{c}$	$\bar{\phi}$	$\bar{\bar{c}} = \bar{\bar{f}}_t$	$\hat{f}_c$	G_c
	[MPa]	[MPa]	[MPa/m]	[MPa/m]	[MPa]	[MPa]	[MPa]	[°]	[°]	[MPa]	[MPa]	[°]	[MPa]	[MPa]	[N/mm]
Avg.	1491	596	14.91	5.96	6.20	0.58	0.23	30.11	28	0.66	0.33	58.15	1.32	6.20	1.00
C.o.V. [%]	24.8	-	-	-	12.2	25.8	-	-	-	-	-	-	-	-	-

In hybrid Finite-Distinct Element Methods, because of nodal compatibility issues, interface springs between adjacent blocks are typically generated at common mesh vertices [19]. Therefore, the number of springs per contact area is a function of the considered tetrahedral FE mesh size, as shown in Fig.2(e). To assess the impact of this aspect on numerical accuracy, results obtained using various FE discretization schemes, characterized by approximate element length (EL) values of 0.05, 0.10 and 0.20 m were compared. The M-DEM simulation results were thus named HW/LW-EL005, HW/LW-EL010 and HW/LW-EL020. For both the considered walls, the overall hysteretic response has been adequately captured by the M-DEMs, as depicted in Fig.3(a)(b). Acceptable agreement between experimental and numerical (absolute) peak base shear BS_p and initial stiffness k_{el} (computed at 10% of BS_p) was found, with only slight differences for different mesh sizes. Similarly, total energy dissipation E_h and ultimate displacement capacities (determined numerically as the displacement at which the panel is no longer able to carry vertical load, and expressed in terms of drift ratio $\delta_{u\%}$) generally compared well. However, for HW models, E_h was noticeably underestimated. The table in Fig.3(e) presents the ratios of numerical predictions to experimental outcomes for four considered parameters: rk_{el}, rBS_p, rE_h and $r\delta_{u\%}$, and indicates whether the model is under-predicts (red color) or over-predicts (light blue color) the observed response. These ratios confirm the observations above regarding the effectiveness of the modeling approach.

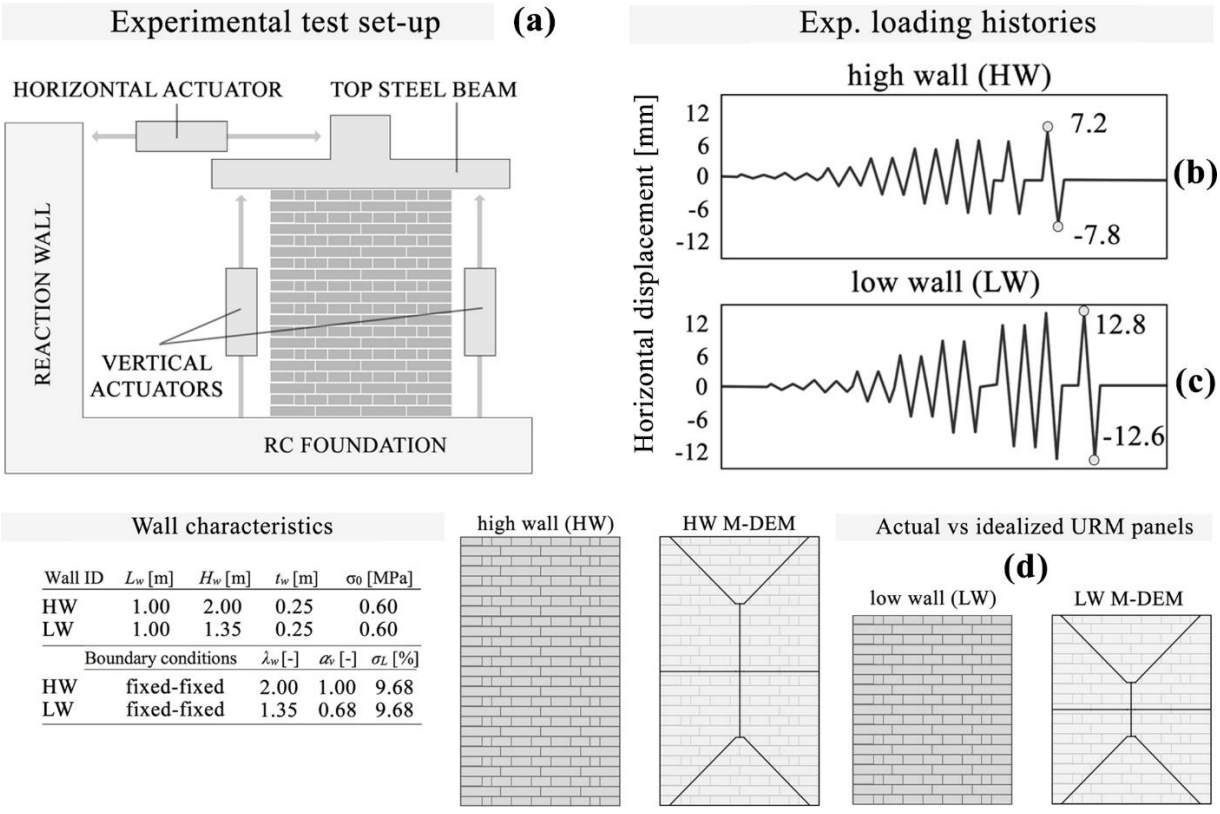

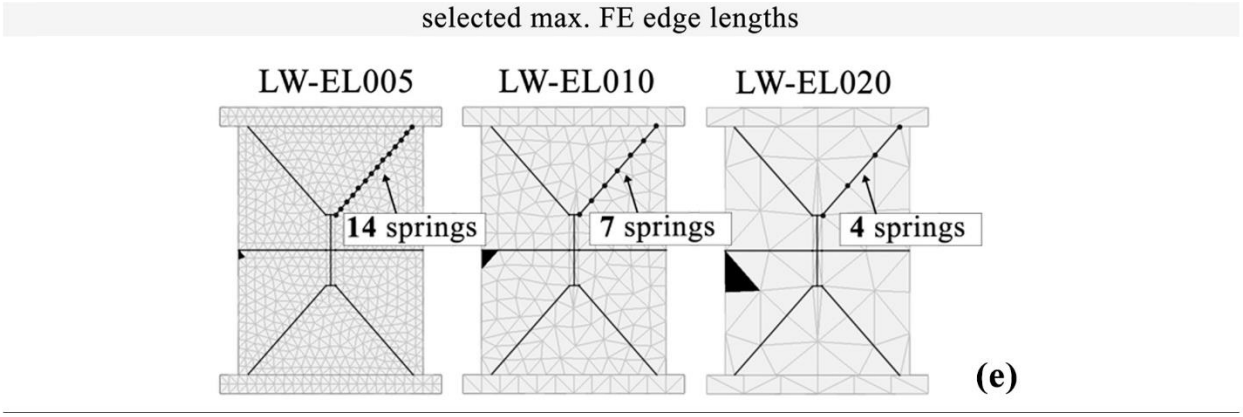

Fig. 2 (a) Exp. configurations, main dimensions and (b) loading protocol for HW and (c) LW specimens, (d) exp. vs num. masonry panel, (e) selected mesh sizes

To further investigating the adequacy of the modeling despite the under-prediction of energy dissipation, a comparison in terms of dimensionless lateral stiffness and energy dissipation ratios is shown in Fig.3(b)(d). These plots are based on two different parameters, defined in Eqs. (6), (7), (8). The first parameter, k_d, represents the ratio between k_i (i.e. the secant stiffness of the *i-th* cycle) and k_{el}, whilst E_d is defined as E_i (i.e. the dissipated energy up to the *i-th* cycle) divided by E_h. Using these simplified indices, as noted by Faella et al. [20], the progressive base shear degradation is implicitly accounted for by the adopted definition of secant (or apparent) lateral stiffness, described in e.g. [21,22]. This secant stiffness, k_i is defined in Eq. (8), where positive/negative values of BS_p and lateral displacements δ are written as $BS_{p,i}^{+}$, $BS_{p,i}^{-}$, $\delta_{,i}^{+}$, $\delta_{,i}^{-}$, respectively.

$$k_d = \left(\frac{k_i}{k_{el}}\right) \quad (6) \qquad E_d = \left(\frac{E_i}{E_h}\right) \quad (7) \qquad k_i = \frac{\left|BS_{p,i}^{+}\right| + \left|BS_{p,i}^{-}\right|}{\left|\delta_{,i}^{+}\right| + \left|\delta_{,i}^{-}\right|} \quad (8)$$

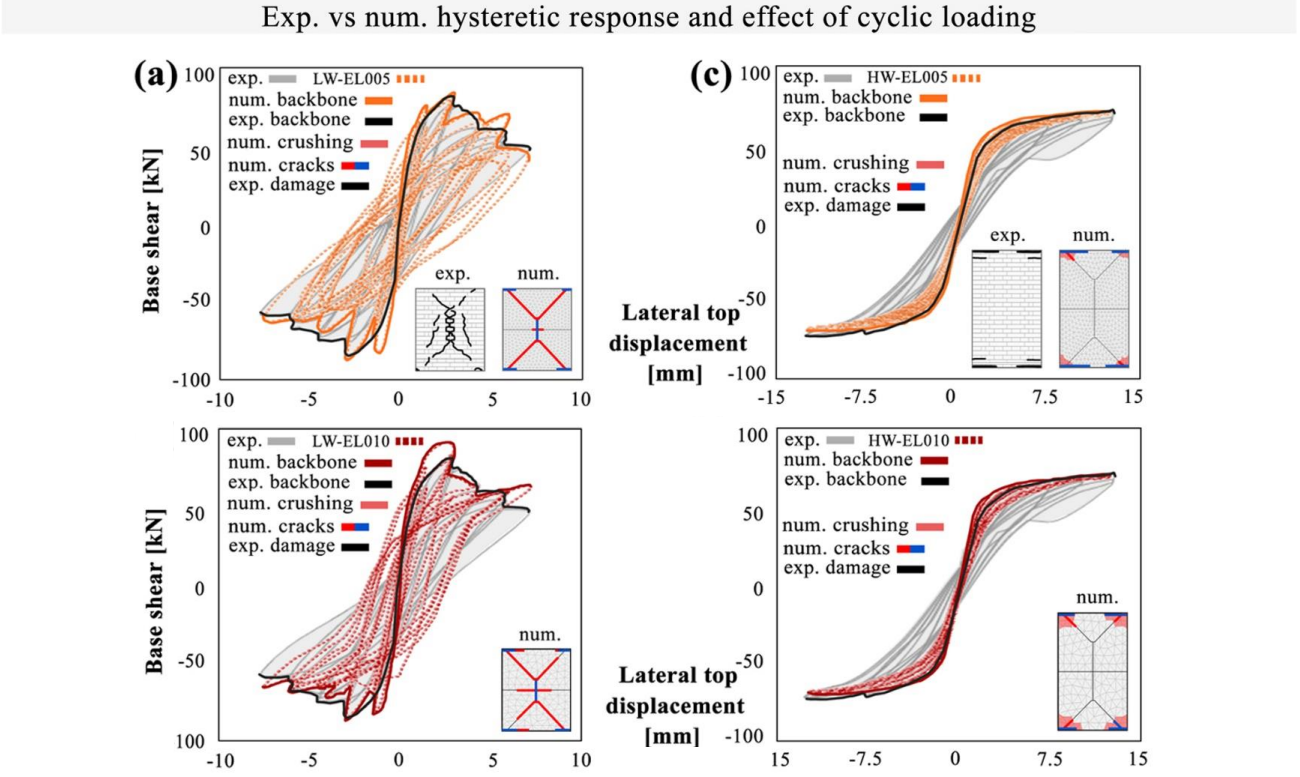

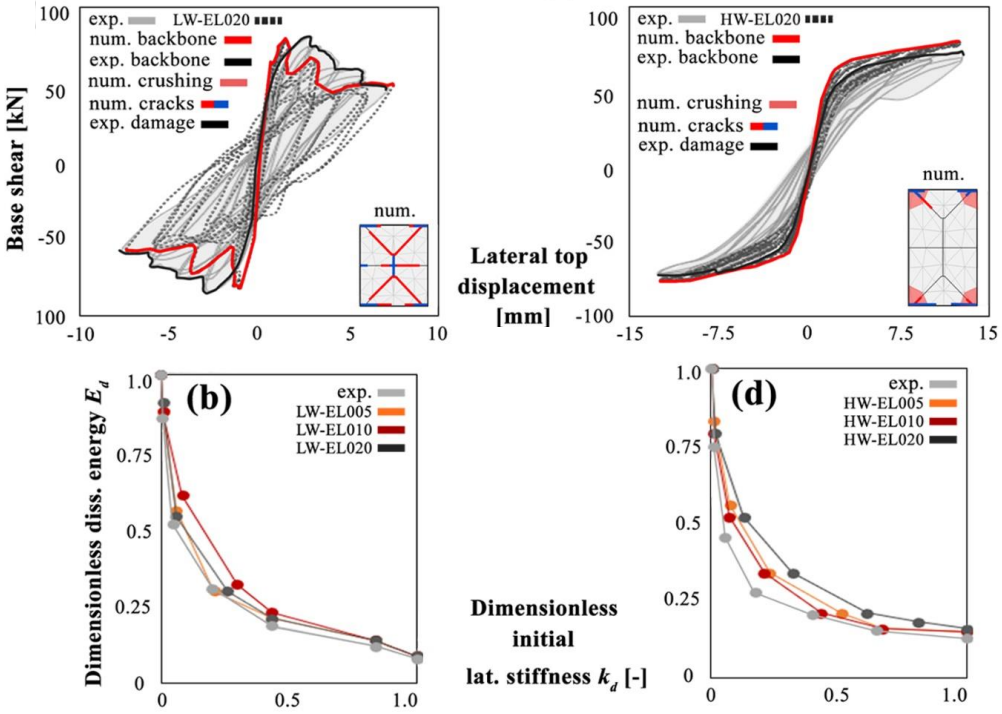

(e) Summary of main results and corresponding num./exp. ratios

	BS_p [kN]	k_{el} [kN/mm]	$\delta_{u\%}$ [%]	E_h [J]	rBS_p [-]	rk_{el} [-]	$r\delta_{u\%}$ [-]	rE_h [-]
LW-EXP.	84.24	90.36	0.60	2251.61	-	-	-	-
LW-EL005	86.77	91.76	0.63	2678.37	*1.03*	*1.02*	*1.05*	*1.28*
LW-EL010	91.34	89.56	0.71	2871.22	*1.08*	*0.99*	*1.18*	*0.95*
LW-EL020	83.82	93.47	0.65	2134.23	*1.00*	*1.03*	*1.08*	*0.92*
HW-EXP.	72.18	43.91	0.65	1768.55	-	-	-	-
HW-EL005	69.29	44.53	0.67	581.76	*0.96*	*1.01*	*1.03*	*0.33*
HW-EL010	70.62	47.48	0.69	567.23	*0.98*	*1.08*	*1.06*	*0.32*
HW-EL020	76.60	45.11	0.78	785.37	*1.06*	*1.03*	*1.20*	*0.44*

Fig. 3 Exp. vs num. hysteretic response and crack pattern and effect of cyclic loading of (a)(b) LW and (c)(d) HW specimens respectively, (e) exp. vs num. main results and associated num. to exp. ratios

The models captured with varying levels of accuracy the interaction between strength and stiffness degradation, as well as the energy dissipation rate. In Fig.3(a)(c), the comparison is also extended to the final crack pattern. For the numerical results, shear (red color) and tension (blue color) lines represent cracks with widths > 0.5 mm. Compressive failure is indicated by the FE regions whose applied stress has exceeded the Feenstra-De Borst strength envelope (light red color). It is worth noting that, even when very coarse mesh schemes are assigned to the FE blocks, a satisfactory representation of the experimentally-observed damage propagation was predicted, for both HW and LW prototypes.

3. Conclusions

The simulation of the global seismic performances of URM buildings still represents an open challenge. Whilst the employment of simplified methods are more suitable for in-plane governed responses, they usually neglect the contribution of out-of-plane modes and their potential interaction with adjacent elements. On the other hand, advanced numerical approaches often require a relatively high computational cost, thus limiting their applicability to the analysis of local mechanisms or to the simulation of reduced-scale arched or dry-joints prototypes. In this paper, a new Macro-Distinct Element Model (M-DEM) for the simulation of the in-plane cyclic response of URM structures is presented and validated through comparison with the outcomes of in-

plane cyclic experimental tests on full-scale URM piers. Each macroelement is representative of either a spandrel or wall element, and constituted by the assembly of internally-meshed FE blocks, connected to each other by nonlinear spring layers, whose layout and equivalent mechanical properties are determined *a priori* as a function of masonry texture and aspect ratio of the considered component. Using this simplified modeling strategy, combined with the implementation of a linearized version of the Feenstra-De Borst compression model for accounting for masonry crushing phenomena, originally not included in the standard formulation of the selected DEM-based code (i.e. 3DEC), both shear and flexure-dominated experimentally-observed hysteretic responses of in-plane tested isolated URM piers, as well as the associated damage propagations, have been duly reproduced. Sensitivity analyses on the influence of FE mesh refinement on numerical accuracy were also conducted, and only minor variations were observed.

4. Acknowledgments

The first author would like to Professor Andrea Penna (University of Pavia, Italy) for his assistance in accessing the test data, as well as for his valuable comments in the early stages of this research regarding both theoretical and practical aspects related to the applicability of the macroelement modeling strategy to the analysis of unreinforced masonry systems.

5. References

[1] Sangirardi M, Liberatore D, Addessi D. Equivalent Frame Modelling of Masonry Walls Based on Plasticity and Damage. Int J Archit Herit 2019;13:1098–109. doi:10.1080/15583058.2019.1645240.

[2] Saloustros S, Pelà L, Cervera M, Roca P. An Enhanced Finite Element Macro-Model for the Realistic Simulation of Localized Cracks in Masonry Structures: A Large-Scale Application. Int J Archit Herit 2018;12:432–47. doi:10.1080/15583058.2017.1323245.

[3] Kallioras S, Graziotti F, Penna A. Numerical assessment of the dynamic response of a URM terraced house exposed to induced seismicity. Bull Earthq Eng 2019;17:1521–52. doi:10.1007/s10518-018-0495-5.

[4] Pantò B, Cannizzaro F, Caliò I, Lourenço PB. Numerical and Experimental Validation of a 3D Macro-Model for the In-Plane and Out-Of-Plane Behavior of Unreinforced Masonry Walls. Int J Archit Herit 2017;11:946–64. doi:10.1080/15583058.2017.1325539.

[5] Lemos J V. Discrete element modeling of masonry structures. Int J Archit Herit 2007;1:190–213. doi:10.1080/15583050601176868.

[6] Cundall PA. A computer model for simulating progressive large-scale movements in blocky rock systems. Proc. Symp. Int. Soc. Rock Mech., vol. 1, Nancy, France: 1971, p. No. 8.

[7] Malomo D, DeJong MJ, Penna A. Distinct element modelling of the in-plane cyclic response of URM walls subjected to shear-compression. Earthq Eng Struct Dyn 2019. doi:10.1002/eqe.3178.

[8] Godio M, Beyer K. Evaluation of force-based and displacement-based out-of-plane seismic assessment methods for unreinforced masonry walls through refined model simulations. Earthq Eng Struct Dyn 2019;48:454–75. doi:10.1002/eqe.3144.

[9] Lemos J V., Campos Costa A. Simulation of Shake Table Tests on Out-of-Plane Masonry Buildings. Part (V): Discrete Element Approach. Int J Archit Herit 2017;11:117–24. doi:10.1080/15583058.2016.1237587.

[10] De Lorenzis L, DeJong MJ, Ochsendorf JA. Failure of masonry arches under impulse base motion. Earthq Eng Struct Dyn 2007;36:2119–36. doi:10.1002/eqe.719.

[11] DeJong MJ, Vibert C. Seismic response of stone masonry spires: Computational and experimental modeling. Eng Struct 2012;40:566–74.

[12] Itasca Consulting Group Inc. 3DEC. Three Dimensional Distinct Element Code 2013.

[13] Malomo D, DeJong MJ, Penna A. Influence of Bond Pattern on the in-plane Behavior of URM Piers. Int J Archit Herit 2019:1–20. doi:10.1080/15583058.2019.1702738.

[14] Magenes G, Calvi GM. In-plane seismic response of brick masonry walls. Earthq Eng Struct Dyn 1997;26:1091–112. doi:10.1002/(SICI)1096-9845(199711)26:11<1091::AID-EQE693>3.0.CO;2-6.

[15] Beyer K, Dazio A. Quasi-static cyclic tests on masonry spandrels. Earthq Spectra 2012;28:907–29. doi:10.1193/1.4000063.

[16] Beyer K. Peak and residual strengths of brick masonry spandrels. Eng Struct 2012;41:533–47. doi:10.1016/j.engstruct.2012.03.015.

[17] Feenstra PH, De Borst R. A composite plasticity model for concrete. Int J Solids Struct 1996;33:707–30. doi:10.1016/0020-7683(95)00060-N.

[18] Anthoine A, Magonette G, Magenes G. Shear-compression testing and analysis of brick masonry walls. Proc. 10th Eur. Conf. Earthq. Eng., vol. 3, Rotterdam, The Netherlands: 1995, p. 1657–62.

[19] Mahabadi OK, Lisjak A, Munjiza A, Grasselli G. Y-Geo: New Combined Finite-Discrete Element Numerical Code for Geomechanical Applications. Int J Geomech 2012;12:676–88. doi:10.1061/(ASCE)GM.1943-5622.0000216.

[20] Faella G, Manfredi G, Realfonzo R. Cyclic behaviour of tuff masonry walls under horizontal loadings. Proc. 6th Can. Mason. Symp., Saskatchewan, Canada: 1992.

[21] Soroushian P, Obaseki K, Ki-Bong Choi. Nonlinear Modelling and Seismic Analysis of Masonry Shear Walls. J Struct Eng 1988;114:1106–19.

[22] Mayes RL, Clough RW. State-of-the-art in Seismic Shear Strength of Masonry: An Evaluation and Review, Report No. EERC 75-21. Berkeley, California: 1975.

